Front. Mech. Eng. 2021, 16(1): 122–132
https://doi.org/10.1007/s11465-020-0603-5

RESEARCH ARTICLE

Adam BENNETT, Nan YU, Marco CASTELLI, Guoda CHEN, Alessio BALLERI, Takuya URAYAMA, Fengzhou FANG

Characterisation of a microwave induced plasma torch for glass surface modification

© Higher Education Press 2021

Abstract Microwave induced plasma torches find wide applications in material and chemical analysis. Investigation of a coaxial electrode microwave induced plasma (CE–MIP) torch is conducted in this study, making it available for glass surface modification and polishing. A dedicated nozzle is designed to inject secondary gases into the main plasma jet. This study details the adaptation of a characterisation process for CE–MIP technology. Microwave spectrum analysis is used to create a polar plot of the microwave energy being emitted from the coaxial electrode, where the microwave energy couples with the gas to generate the plasma jet. Optical emission spectroscopy analysis is also employed to create spatial maps of the photonic intensity distribution within the plasma jet when different additional gases are injected into it. The CE–MIP torch is experimentally tested for surface energy modification on glass where it creates a super-hydrophilic surface.

Received May 7, 2020; accepted August 3, 2020

Adam BENNETT
Surface Engineering and Precision Institute, Cranfield University, Cranfield MK43 0AL, UK

Nan YU (✉), Fengzhou FANG (✉)
Centre for Micro/Nano Manufacturing Technology (MNMT-Dublin), University College Dublin, Dublin D04 V1W8, Ireland
E-mails: nan.yu@ucd.ie; fengzhou.fang@ucd.ie

Marco CASTELLI
Manufacturing Technology Centre (MTC), Coventry CV7 9JU, UK

Guoda CHEN
Key Laboratory of E&M, Ministry of Education & Zhejiang Province, Zhejiang University of Technology, Hangzhou 310014, China

Alessio BALLERI
Centre for Electronic Warfare, Information and Cyber, Cranfield University, Shrivenham SN6 8LA, UK

Takuya URAYAMA
Adtec Plasma Technology Co., Ltd., Fukuyama, Hiroshima 712-0942, Japan

Keywords microwave induced plasma, spectrum analysis, surface modification

1 Introduction

Ultra-smooth surface processing can be realized by utilising mechanical [1], electrochemical mechanical [2], dry chemical process [3], or by energy beam [4] technology. Previous plasma figuring of silicon based optical surfaces has been undertaken using a radio frequency plasma jet at atmospheric pressure. Inductively coupled plasma technology was demonstrated on large optical surfaces made of ultra-low expansion glass and fused silica using reactive plasma jets [5]. Capacitively coupled microwave plasma and capacitively coupled plasma technologies have also demonstrated form correction of optical surfaces [6,7]. In other plasma chemistry applications microwave induced plasma (MIP) has become the principal microwave plasma technology [8]. MIP generates plasma through the inductive transfer of energy from standing waves within a resonator, where a dielectric tube is located. The design typically employed for discharging atmospheric pressure plasma jets involves the use of a coaxial electrode to launch the microwaves into the gas.

Recently, innovative applications using atmospheric pressure plasma have been developed in the medical sector for the sterilisation of wounds [9] and as a surgical cutting tool [10], in the water sector for the cleaning of contaminated water supplies [11], and in the surface engineering sector for increasing surface free energy, which improves surface bonding [12]. Micro plasmas range between micrometre and millimetre in size and generally operate at atmospheric pressure. Micro plasma torches have been used as ultra-violet sources [13], for nanomaterial processing [14], material synthesis [15], chemical analysis [16], electromagnetic physics [17], and engine combustion [18].

MIP systems couple microwaves into gas to generate plasma. Therefore, to gain insight into the fundamental mechanisms that underpin the plasma torch operation, characterisation of the electromagnetic field before coupling with the gas and characterisation of the resulting plasma jet was performed. When a coaxial electrode microwave induced plasma (CE–MIP) torch is in operation, the reflected power within the system is reduced to 0 W enabling all of the power, theoretically, to be deployed to sustain the plasma discharge. This is achieved by the use of a tuning element between the microwave generator and the coaxial electrode [19]. Typically, vector network analysis [20] has been used for the determination of the magnitude and phase of the microwave signals passing through the tuning element, and hence the characterisation of the reflected power. However, vector network analysis only characterises the microwave energy in the circuit and provides no information on the emitted microwave electric field from the electrode [21]. This study adapted a spectrum analysis technique to give detailed information on the microwave electric field that was emitted into the primary gas flow. This was important as the surface roughness and topography of the coaxial electrode would affect the amount of the electric field emitted that can then couple with the plasma [22]. Conversely, optical emission spectroscopy (OES) is an effective characterisation method for analysing plasma jets [23]. A typical setup consists of microwaves passing through a fused quartz tube and then ionising an argon gas flow. The OES instrument consists of a spectrometer that is attached to a lens, which is focused perpendicular to the discharge direction of the plasma jet. This allows for the intensities of the different wavelengths being emitted by the plasma jet to be recorded so that a spatial distribution can be obtained [24].

Prior to this study, Bennett et al. [25] demonstrated surface cleaning of concentrating solar power (CSP) mirrors using an air plasma array. The air plasma jet removes the sand deposited on the mirror surfaces, by targeting the physical and chemical bonding aspects of the sand on glass surfaces. The CSP mirror is also required to be modified with super-hydrophilic or super-hydrophobic properties (depending on sand grain size), which in turn will make it self-clean at night when there is a high level of humidity present in the air.

Surface modification is required to make surfaces super-hydrophilic or super-hydrophobic. Williams et al. [12] demonstrated argon plasma temporarily makes a super-hydrophilic surface on steel, which results in improved bonding of components; however, more permanent super-hydrophilic or super-hydrophobic surfaces may be produced by using reactive species. Previous work undertaken by Bennett et al. [26] demonstrates that the surface of crystalline quartz may have its surface roughness increased from 1.5 to 3.5 nm Sq by the application of an argon and fluorine plasma at atmospheric pressure. This level of surface roughness increase will significantly increase the hydrophobicity of the surface.

2 Design of CE–MIP torch

Figure 1(a) shows a typical plasma surface treatment process using an MIP torch, supplied by Adtec Plasma Technology Co., Ltd., Japan. A microwave generator was connected to a coaxial cable that was in turn connected to a tuning element. The tuning element was connected directly to a resonant cavity. The end of the resonant cavity had the option of having a nozzle attached, as shown in Fig. 1(b). Originally, the CE–MIP system had a nozzle attached to the end of the plasma torch but could not inject secondary gas. The key elements in this design were located within the resonant cavity, where a coaxial electrode was

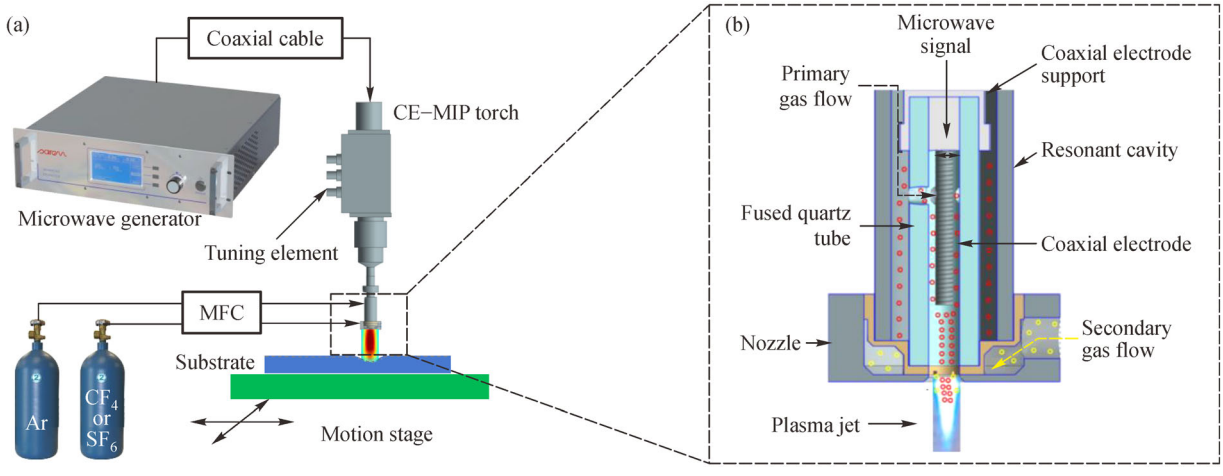


Fig. 1 Schematic of the plasma surface processing. (a) Experimental setup of plasma processing using CE–MIP torch; (b) working principle of the CE–MIP torch for reactive plasma jet generation. CE–MIP: Coaxial electrode microwave induced plasma; MFC: Mass flow controller.

surrounded by a quartz tube, as shown in Fig. 1(b). The holes in the fused quartz tube allow the primary gas to flow into the quartz tube where it couples with the microwave energy to generate the plasma discharge. The nozzle design shown in Fig. 2 highlights the divergent nozzle's ability to inject secondary gas downstream of the main plasma jet that was discharged from the resonant cavity.

The CE–MIP torch in this study uses a bespoke coaxial electrode design. The electrode is made from a 1 mm wide material. This bespoke surface topography, which required significant effort to machine into the electrode material, enables the plasma torch to discharge a spiralling plasma jet and thus gives stability to the plasma jet discharge. Furthermore, the surface topography creates a higher electric field intensity, which results in a higher coupling efficiency with the plasma: The plasma is generated near the nozzle and not along the entire surface of the coaxial electrode.

The microwave power was transferred via a tuning element into the coaxial electrode, which was at the centre of the resonant cavity symmetrically dissipating the energy into the plasma. The tuning element consists of three resonant stubs in the transmission line, where one end of the stubs is left as an open circuit. Neglecting transmission line losses, the input impedance of the resonant stubs is purely reactive, and the physical length of the resonant stubs was chosen for inductive coupling. The length was calculated by taking the input impedance equation for an open-circuit stub, which is given as [27]

$$Z_{oc} = -jZ_0\cot(\beta l), \tag{1}$$

and choosing the condition when $\cot(\beta l)$ is negative, thus yielding:

$$l = \frac{1}{\beta}\left[(n+1)\pi - \cot^{-1}\left(\frac{\omega L}{Z_0}\right)\right], \tag{2}$$

where j is the imaginary unit, Z_0 is the characteristic impedance of the line, β is $2\pi/\lambda$, which is defined as the phase constant of the line, l is the physical length of the line, L is inductance, ω is the angular frequency, and n is an integer multiple of the fundamental resonant frequency.

The setting of the resonant stubs at the correct lengths enables the microwave power being sent into the plasma to be optimised, which reduces the power reflected into the generator. In this study argon plasma was discharged and the reflected power was reduced to less than 0.3%. The microwave emission around the coaxial electrode was found to be uniform and axis symmetric; and, effectively no microwave leakage occurred from the resonant cavity even when the microwave energy was being emitted without having any gas flow to turn into plasma. Therefore, the CE–MIP torch was deemed safe and suitable for ultra-precision plasma surface treatment experiments.

Furthermore, the original CE–MIP torch was designed to operate in non-confined mode, which is required for a

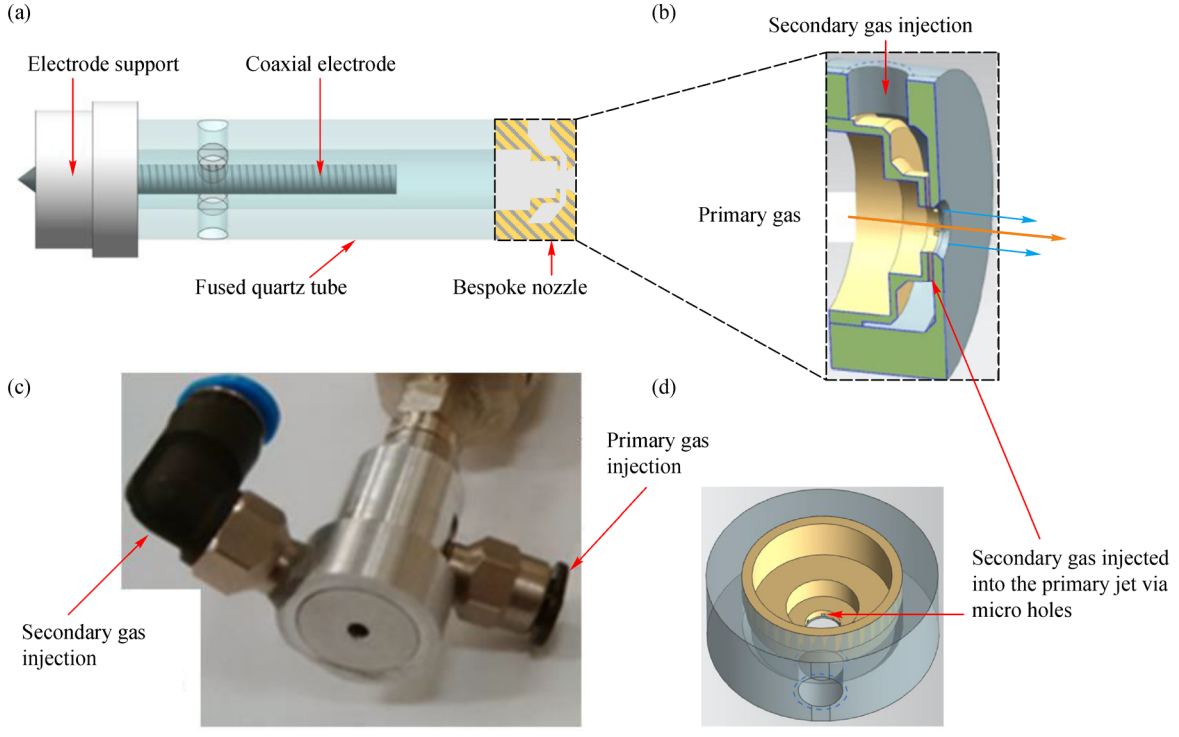


Fig. 2 Design of a divergent nozzle with microfluidic channels for the injection of secondary gases. (a) Schematic of the CE–MIP torch; (b) cross section of the bespoke nozzle; (c) CE–MIP torch nozzle with two gas injection tubes; (d) CAD model of the nozzle design, showing the micro holes' distribution. CE–MIP: Coaxial electrode microwave induced plasma.

plasma jet discharging beyond the nozzle. This modification to the MIP torch underpinned the following experimental work carried out in this study. The design and test of the CE–MIP torch will be addressed in the following sections, focusing on the nozzle design and the microwave spectrum analysis for the torch.

2.1 Nozzle design

The bespoke nozzle was designed and fabricated, with the aim of injecting reactive gases into the argon plasma jet, which was operated at atmospheric pressure. Reactive gases, such as carbon tetrafluoride or sulphur hexafluoride, need to be injected downstream of the electrode to avoid electrode degradation. Unlike the previous de-Laval nozzle designs in ICP torches [28,29], the nozzle in this study is divergent only. The nozzle design achieves this by injecting the secondary gas into the main plasma below the plasma generation region. The secondary gas is injected through four micro holes (Figs. 2(b) and 2(d)) positioned at equally separated locations around the axis of the plasma jet, which is a crucial design consideration for maintaining plasma jet stability and equal spatial distribution of the secondary atomic species within the main plasma discharge. Figure 2 shows the construction of the plasma torch and the bespoke nozzle.

2.2 Microwave spectrum analysis

The coaxial electrode in a CE–MIP torch behaves as an antenna emitting microwave energy. The directionality of the energy being emitted by the coaxial electrode, therefore, determines the point in space where the electric field density is at a maximum and hence where microwaves would couple with gas to generate plasma. To determine the directionality of the energy being emitted from the coaxial electrode, a microwave polar plot was obtained using a modified antenna characterisation experiment. Figure 3 shows the experimental setup for microwave spectrum analysis.

Firstly, the tuning element with coaxial electrode attached, is mounted on a LT360 precision turntable, within a RADAR microwave anechoic chamber. Microwaves were emitted from the coaxial electrode at a constant forward power of 1 W, at a fixed frequency of 2.45 GHz. The microwaves travelled 1.4 m through the air in the anechoic chamber and were recorded by a receiving antenna at the other end of the chamber. The receiving antenna was connected to an Anritsu signal analyser, which was used to measure and analyse the microwaves. The distance of 1.4 m was calculated from the Far-Field Range calculation [30]. The precision turntable moved the coaxial electrode from –90° to + 90° pitch, starting with the coaxial electrode axis parallel with the receiving antenna and ending at a normal to it. The coaxial electrode was rotated and at 1° intervals the received intensity was recorded, where the receiving antenna was set to receive the horizontal polarisation of the electric field as shown in Fig. 4.

Secondly, the quartz tube was mounted around the coaxial electrode and the experiment was repeated.

The test was followed by mounting the resonant cavity next and then the bespoke nozzle. The previous experiments were conducted where the precision motion stage

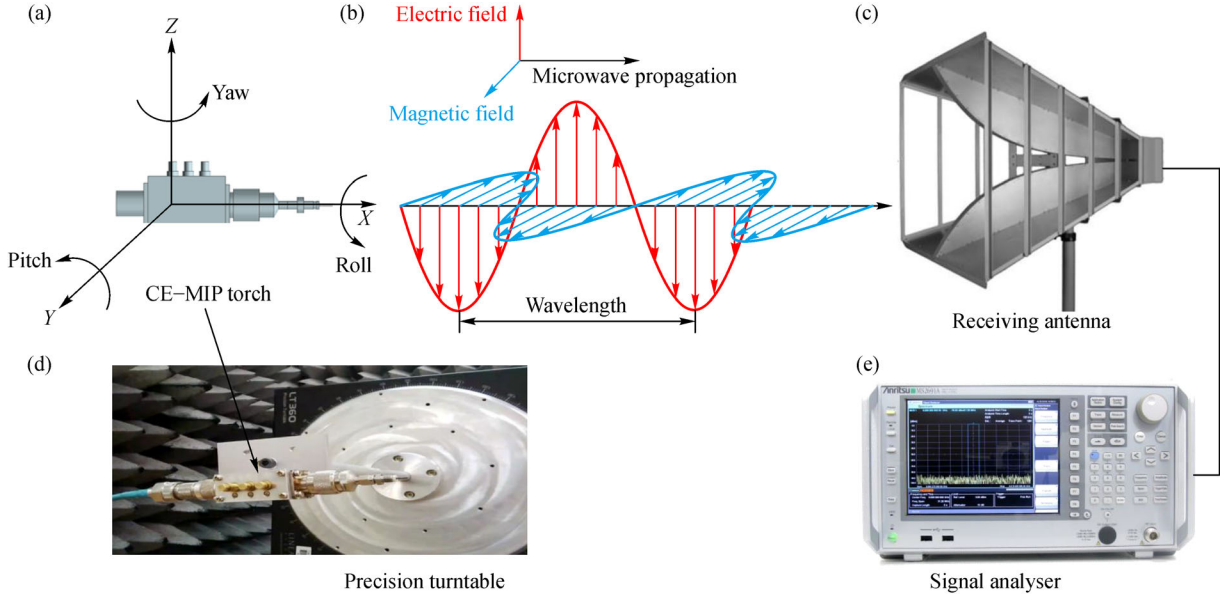


Fig. 3 Experimental setup for microwave spectrum analysis. (a) Six degrees of freedom of the CE–MIP torch; (b) microwave propagation; (c) receiving antenna; (d) CE–MIP torch mounted on a precision motion stage; (e) signal analyser. CE–MIP: Coaxial electrode microwave induced plasma.

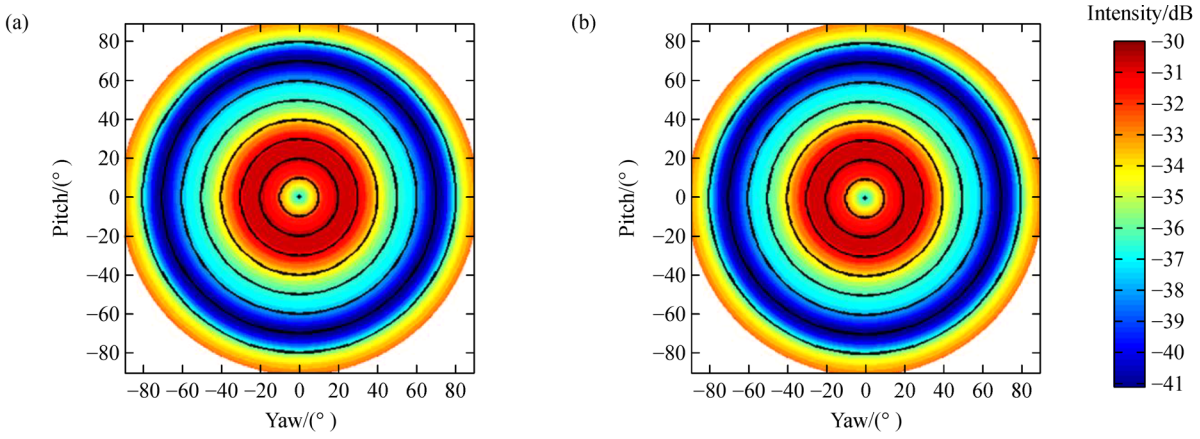


Fig. 4 Emission intensity from the receiving antenna. (a) Horizontal and (b) vertical polarisations.

rotated the coaxial electrode from –90° to + 90° pitch. To confirm that the electric field being emitted was axis symmetric, the above set of experiments where repeated where the setup was rotated from –90° to + 90° yaw.

Finally, the polarisation of the receiving antenna was considered. All of the previous experiments rotating the setup through pitch and yaw, where conducted with the receiving antenna orientated to receive the horizontal polarisation of the electric field. To ascertain the polarisation of the electric field, the pitch and yaw experiments were repeated with the receiving antenna in the vertical polarization state, rotated 90° relative to the horizontal polarisation.

2.3 Spectrum analysis results

The microwave polar plot was generated by measuring the received intensity, relative to the emitted intensity, at each point in space, in the region of the emitting coaxial electrode. The *X*-axis corresponds to the yaw and the *Y*-axis corresponds to the pitch of the emitting coaxial electrode; where the axes are aligned with the receiving antenna so that (0, 0) corresponds to the position shown in Fig. 3, where the coaxial electrode axis was parallel with the receiving antenna. The received intensity is shown as a measured loss in negative dB and is a logarithmic scale.

2.3.1 Axis symmetry and polarization effect

Figure 4 shows the effect of rotating the coaxial electrode through 180° yaw and 180° pitch, when the receiving antenna was set to receive the horizontal and vertical polarizations, respectively. The results clearly show that the emission of the electrode was axis symmetric. Considering the length of the coaxial electrode was 12 mm, which was an order of magnitude smaller than the emitting wavelength, one would expect that the emission had axis symmetry. However, this was an important result as it showed that the coupling of the microwave electric field with the plasma can be uniform around the electrode. Furthermore, this result also indicated that the coupling would occur near the end of the electrode, which was at the nozzle end of the plasma torch and corresponded with a plasma jet operating in non-confined mode [31]. When subtracting Fig. 4(a) from Fig. 4(b), the result was zero, within the error of the measurement system; and therefore, it was concluded that the coaxial electrode emitted uniform and circular polarised microwave energy. The result that the emission of the electrode was axis symmetric and uniformly polarised meant that the energy being emitted into the plasma was uniform and therefore that the plasma coupling around the electrode should be uniform.

2.3.2 Measured electric field with different MIP torch configurations

Figure 5 shows how the energy being received varied when the various additional components of the torch assembly were added. These additional experiments were conducted to determine the benefit of enclosing the coaxial electrode within a quartz tube and to ascertain whether any microwave leakage occurred from the fully assembled plasma torch: Even when no plasma was being discharged.

Note that Figs. 4 and 5(a) show the same result in different measures. The results in Fig. 5 were all displayed with the same intensity range: Covering the entire range measured in all experiments. This approach was taken to make the results easily comparable for the reader. Figure 5(a) shows the result when only the coaxial electrode was used to sweep through yaw and pitch, Fig. 5(b) shows the result when the quartz tube was mounted around the coaxial electrode and the experiment was repeated, Fig. 5(c) shows the result when the chamber was mounted, and Fig. 5(d) shows the result when the bespoke nozzle was added onto the whole torch.

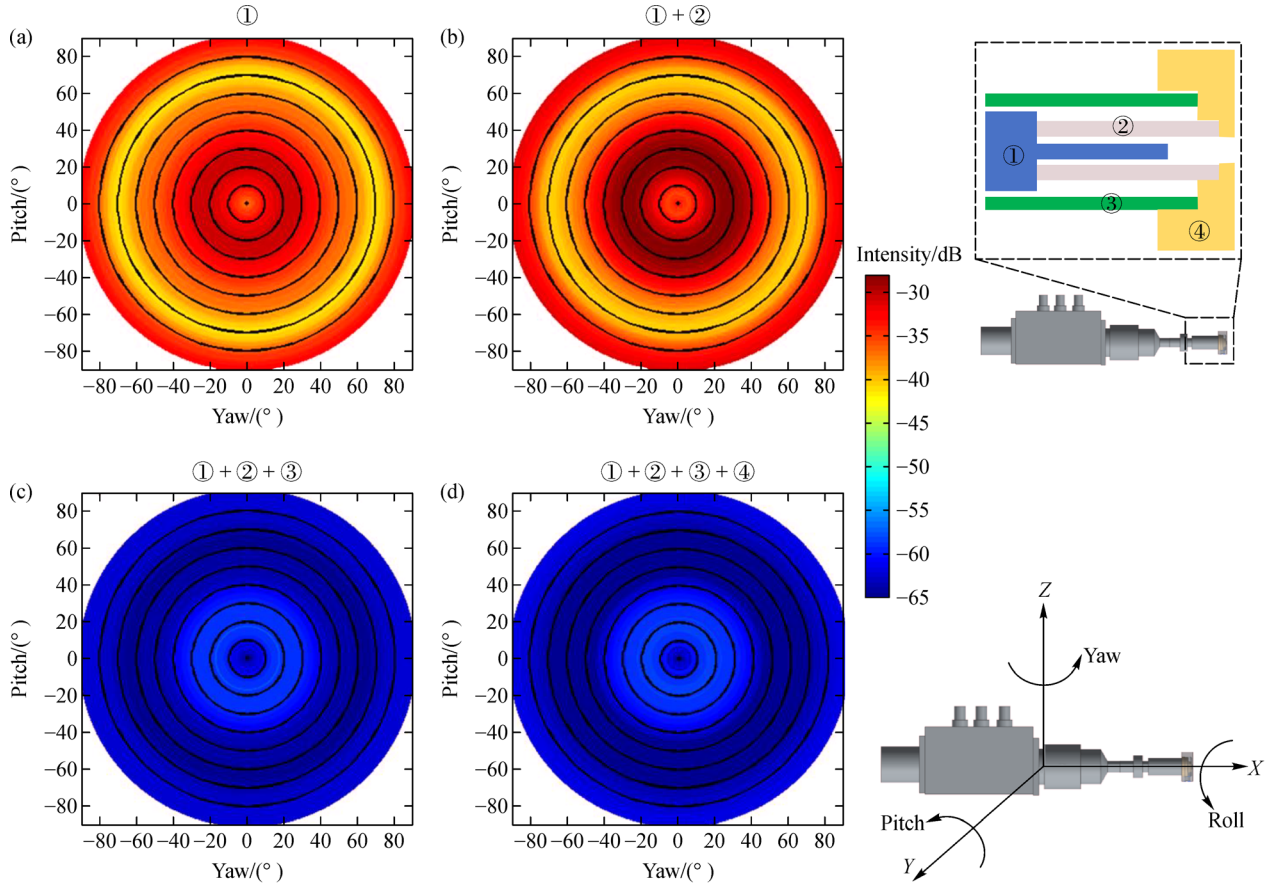


Fig. 5 Measured electric field with different CE–MIP torch configurations: (a) Coaxial electrode only; (b) coaxial electrode with quartz tube; (c) coaxial electrode with quartz tube plus a chamber; (d) whole MIP torch attached with the bespoke nozzle. Note: The MIP torch contains four elements, as shown in this figure, ① coaxial electrode, ② quartz tube, ③ resonant chamber, and ④ bespoke nozzle. The adjustment of pitch and yaw are given in this figure. CE–MIP: Coaxial electrode microwave induced plasma; MIP: Microwave induced plasma.

2.3.3 Analysis on the measured electric field

As the emission of the coaxial electrode was shown to be axis symmetric and uniformly polarized, the different torch configurations were compared by analysing a single sweep from 0° to 90° in yaw. Figure 6 shows how the relative microwave electric field varies with the different torch configurations. The regions of lower loss, lower negative intensity, represent the regions of higher electric field density and show the regions where the microwaves would couple with the plasma.

There are two distinct regions of higher electric field density: One around the 10° to 30° range, where the intensity of the 'electrode & quartz tube' arrangement was as high as –28 dB; and one at the 80° to 90° range, where the intensity of the same arrangement was as high as –31 dB. This implies that the coaxial electrode may generate plasma at one of two distinctly different regions, either near the end of the coaxial electrode or near the base. The region of interest for a plasma torch is the former, as the plasma needs to be generated at the end of the resonant cavity such that it discharges out of the nozzle in the form of a plasma jet operating in non-confined mode.

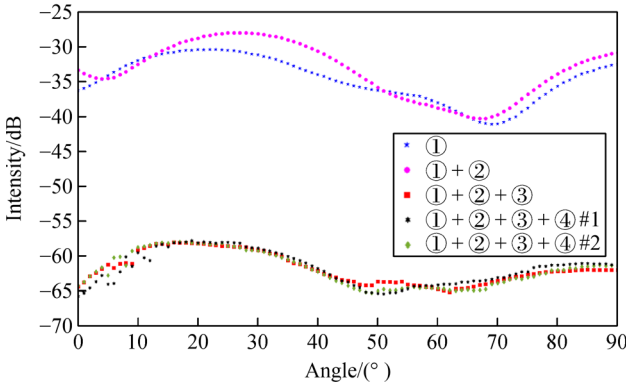


Fig. 6 Measured electric field with different CE–MIP torch configurations. ① Coaxial electrode, ② quartz tube, ③ resonant chamber, and ④ bespoke nozzle with two versions # 1 and # 2.

3 OES characterisation of the CE–MIP torch

To develop spatial maps of the photonic intensity distribution within the plasma jet when different additional gases were injected into the CE–MIP torch, OES characterisation was carried out in this study. Photonic intensity spatial maps were generated, by recording the intensities of the different photons that were emitted, from the relaxation of high energy level electrons in the dissociated plasma jet. The plasma jet was discharged from the CE–MIP torch, which was operated at atmospheric pressure. The microwave plasma torch used argon as a main carrier gas. Argon (Ar), sulphur hexafluoride (SF_6), or carbon tetrafluoride (CF_4) secondary gas was injected into the plasma jet via the bespoke nozzle. A comparison of the photonic intensity spatial maps is given and discussed.

3.1 OES experimental setup

A solid-state microwave generator was connected to a coaxial cable, which was in turn connected to the CE–MIP torch. The plasma torch was installed into a fixed position within a precision computer numerical control (CNC) machine. Existing within the machine was a precision motion stage, which could be moved to a place in 3D space within ±10 μm. Upon the precision motion stage was placed an Ocean Optics HR4000 Spectrometer for OES characterisation of the plasma jet. The microwave power was set to 15 W, as this was the maximum safe value for the CE–MIP micro torch. The operational frequency was 2.45 GHz as this was the fixed value of the solid-state generator. The main gas flow was set to 1 L/min, as this was comparable with literature and the injected secondary gas into the nozzle, where applicable, was set to 0.01 L/min. A schematic diagram of the plasma torch in operation is shown in Fig. 1(b), which clearly shows the main/primary gas flow into the resonant cavity, and the secondary gas flow into the bespoke nozzle.

3.2 Optical emission spectroscopy results

The microwave power and the main gas flow were set, and the plasma was ignited. Figure 7 shows four photon emission intensity spatial maps. Figure 7(a) shows the integrated photon intensities before the additional gas was injected into the bespoke nozzle and Fig. 7(b) shows how the intensity map changed when an additional 0.01 L/min of argon gas was injected downstream of the main plasma jet discharge. This comparison between Figs. 7(a) and 7(b) indicates that the addition of argon gas into an argon plasma jet increases the photons emitted, which corresponds to an increased average electron temperature within the plasma jet. The Ar gas injected via the nozzle was incident upon the outer layers of the plasma jet where the microwave energy couples with the plasma through the skin effect. This could be the reason for the relatively significant increase of energy recorded for only a 1% increase of Ar.

Figure 7(c) presents how the Ar intensity map changed when SF_6 was injected downstream of the main argon plasma jet at a flow rate of 0.01 L/min. No fluorine emission was measured. The comparison between Figs. 7(a) and 7(c) show that the addition of 1% SF_6 decreases the photons emitted, which corresponds to a decreased average electron temperature within the plasma

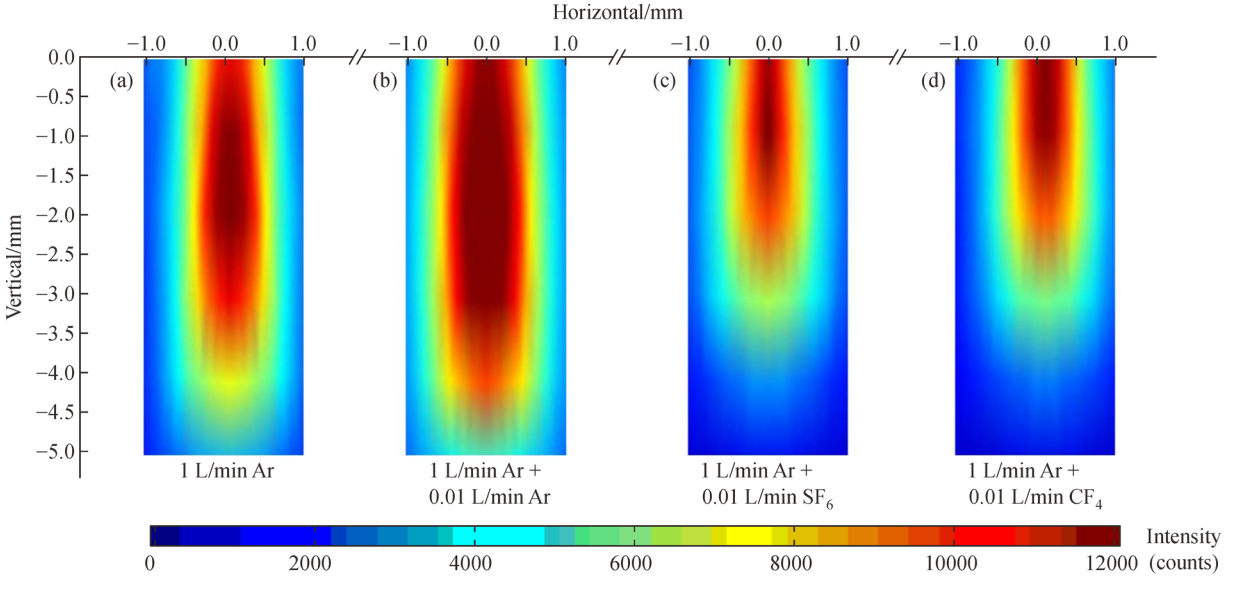


Fig. 7 Photon emission intensity spatial maps with different gas injections: (a) Main gas = 1 L/min Ar; (b) main gas = 1 L/min Ar, and secondary gas = 0.01 L/min Ar; (c) main gas = 1 L/min Ar, and secondary gas = 0.01 L/min SF_6; (d) main gas = 1 L/min Ar, and secondary gas = 0.01 L/min CF_4.

jet. Fluorine molecules are prone to weakening a plasma jet discharge, due to electron attachment, and this can result in plasma extinction. Furthermore, the excitation of the molecules' electron energy levels consumes energy. Therefore, electron energy is significantly more dissipated via fluorine excitation processes compared to argon.

In the previous experiment it was observed that there was not enough energy in the plasma to dissociate the SF_6 molecules. However, CF_4 gas dissociation occurs at lower energies when at room temperature [32]. Therefore, it was also logical to investigate the injection of CF_4 molecules. Figure 7(d) shows how the intensity changed when CF_4 was injected downstream of the main plasma jet at a flow rate of 0.01 L/min. Again, no fluorine emission was measured. Similarly to Fig. 7(c), it also shows that the addition of 1% CF_4 into the outer layers of the Ar plasma jet decreases the photons emitted, which corresponds to a decreased average electron temperature within the plasma jet.

3.3 Optical emission spectroscopy analysis

The plasma maps in Fig. 7 show how the photonic energy being emitted from the argon atoms in the plasma jet decrease when the SF_6 or CF_4 was injected. There were also no additional wavelengths detected anywhere in the maps. Therefore, it is concluded that this CE–MIP micro torch is not suitable for plasma etching of optics, because no reactive atoms could be generated. A higher power system is required.

The photonic energy density being emitted from the plasma jet corresponds to the electron density, as the photons are emitted from electron transitions to lower energy levels. To determine the relative electron density cross section of the plasma jet, a cross section, of a dominant near infrared wavelength was taken. Figure 8(a) shows the relative density from photons of wavelength 801.5 nm distributed across the plasma jet. The cross section was taken at 1 mm downstream from the nozzle, where the plasma jet was most stable. A pure argon plasma jet was discharged and no secondary gas was injected.

The injection of additional gases, into the outer layers of the plasma jet discharge was investigated further. The comparison of different secondary gases in Fig. 8(b) shows the change in the relative density from photons of wavelength 801.5 nm. Data acquisition was undertaken at the centre of axis, 3.3 mm downstream from the nozzle, because it was the region in space with the largest range of different values for the different secondary gases. The maximum microwave power was limited to 15 W due to the size and surface structure of the coaxial electrode and at this low power there was not enough energy to cause dissociation of CF_4 or SF_6 molecules. The injection of CF_4 or SF_6, however, did result in the relative intensity of the 801.5 nm photons reducing from 12000 to 7000 counts. This reduction in near infrared energy is due to the absorption from the injected secondary gases.

4 Surface energy modification of CSP glass

The CE–MIP torch was used for surface treatment of mirrors, where five identical CSP glass samples were selected for this experiment. The experimental setup for plasma treatment and surface measurement is shown in Fig. 9. Each sample was placed, sequentially, on the precision motion stage, which enabled the samples to be moved under the plasma torch in a raster-scanning motion

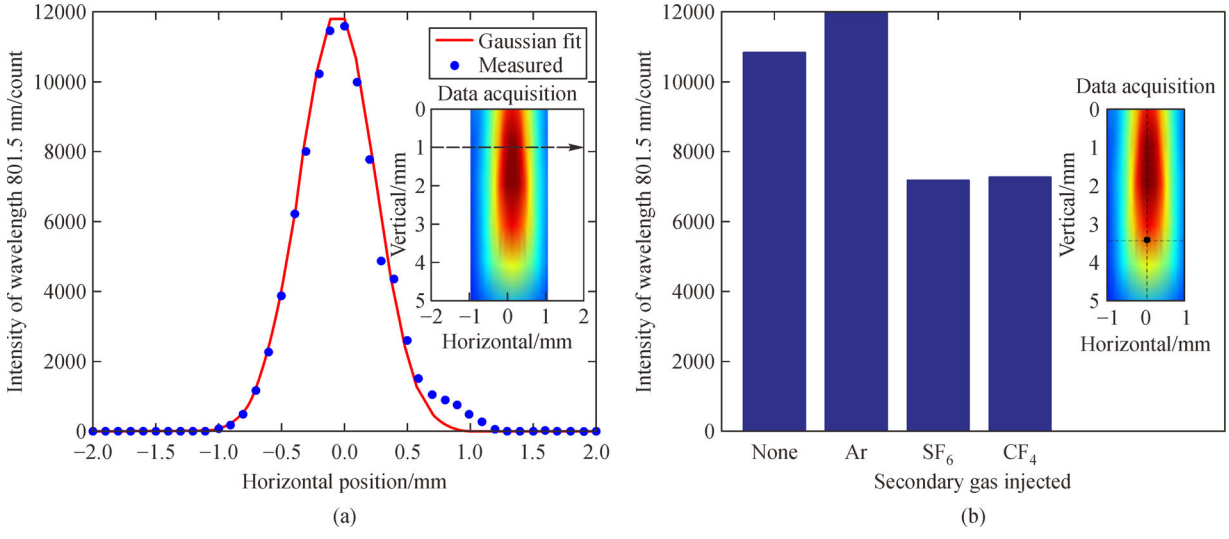


Fig. 8 Intensity of wavelength 801.5 nm. (a) Intensity of plasma jet cross section, with data acquisition at 1 mm downstream from the nozzle; (b) comparison of the intensity of the plasma jet with different secondary gases injected. The plasma jet analysis locus is 3.3 mm downstream from the nozzle at the centre of axis.

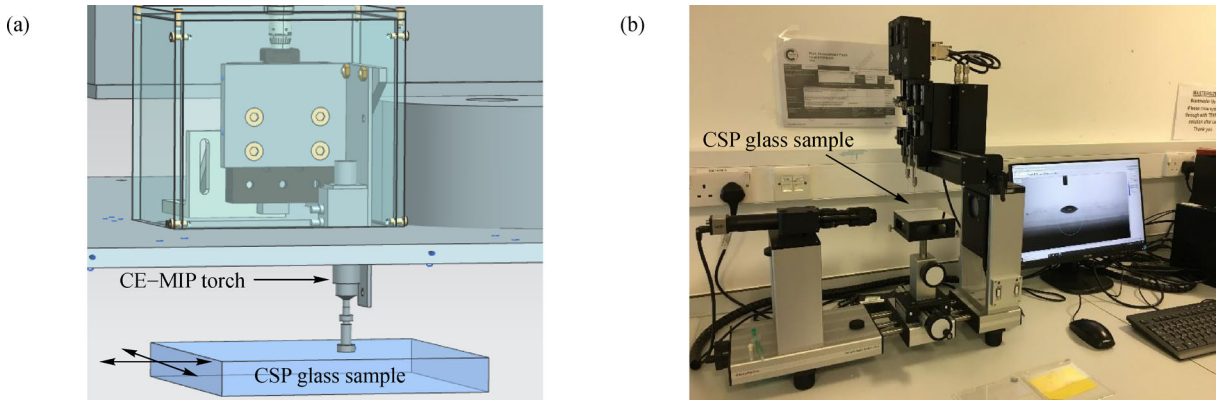


Fig. 9 Surface energy modification experiment and measurement. (a) Experimental setup for CE–MIP treatment of CSP glass, located on a X–Y motion stage; (b) measurement machine for the water contact angle on the CSP glass samples. CE–MIP: Coaxial electrode microwave induced plasma; CSP: Concentrating solar power.

with 1 mm separation between passes, hence enabling a uniform treatment of the surface. The power was set to 15 W and the argon gas flow was set to 1 L/min. The stand-off distance between the plasma torch nozzle and the glass sample was 10 mm. A different speed was used for each sample. The water contact angles were measured by using a contact angle goniometer. The water contact angle on the glass sample surface before plasma treatment was 57°±1°. They were then re-measured on the processed sample surface. Each sample was processed and re-measured three times to show the effect of further processing. Finally, the aging of the contact angles was measured: Every hour for the first 6 h, then after 12 and 24 h, and then daily for a total of 8 d.

Figure 10(a) shows experimental results demonstrating that the water contact angle on the surface of the mirrors was reduced from initially circa 57° to less than 9°. These results also show that the contact angle was reduced by greater amount when the plasma jet was moved at a slower speed or with repeated passes. The contact angle was reduced to circa 3° for a single pass at 1 m/min and this reduced down to 1° after three passes. The reduction in the contact angle of water on the mirrors' surfaces corresponds to an increase in the mirrors' degree of self-cleaning and this is due to an increase in the surface energy of the mirror surfaces.

Figure 10(b) shows how the super-hydrophilicity ages with respect to time, on the CSP mirror samples that were plasma processed at a speed of between 1 and 5 m/min, with three passes for each test. The results indicate that the super-hydrophilic effect lasts for a couple of days and that after eight days the hydrophilic effect had reduced to a contact angle of circa 30°. The stability of the torch was tested, using OES, in this study to ensure repeatable results (with deviation of 0.5°) and the MIP torch performed constantly over a 12-h period, which gives confidence to the surface energy modification repeatability.

5 Discussion

As it is implied in Section 2.3.3, the coupling region of interest for a CE–MIP plasma torch is near the end of the coaxial electrode, where it discharges plasma out of the

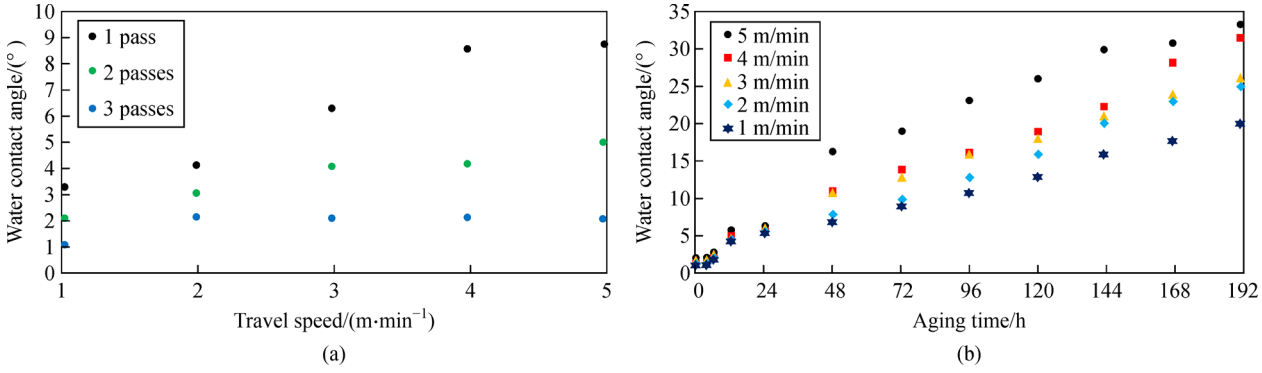


Fig. 10 Measurement result of the modified glass surface. (a) Water contact angle versus plasma torch travel speed, for a different number of passes; (b) water contact angle versus aging time, with plasma torch travel speed varying between 1 and 5 m/min. All samples were plasma processed with three passes.

nozzle in the form of a non-confined mode plasma jet. However, the results in Fig. 6 show that the plasma may also form inside the fused quartz tube in confined mode, which is useful for chemical analysis [31]. This experimental setup was designed to measure the far field emission from the coaxial electrode. The measurements made when the nozzle was attached showed that there was no microwave leakage; however the measurements do not give information on how the microwave electric field is affected by the presence of the nozzle and hence how the nozzle affects the microwave–plasma coupling. The attachment of the nozzle might have the effect of flattening out the maximum electric intensity emitted from the coaxial electrode and consequently might cause the microwave–plasma coupling to occur more uniformly throughout the quartz tube.

The CE–MIP torch was successfully characterised and tested in surface modification experiments. The emission profile in Fig. 8(a) was very close to a Gaussian distribution, which means the plasma jet discharge is stable. The deviation from Gaussian occurred on the right-hand edge of the scan in the X direction. This location corresponds to the side of the plasma jet that was facing the rear of the precision CNC machine, where an air extraction fan was situated. It is concluded that the air flow generated from this air extraction fan was responsible for the deviation from Gaussian of the energy within the plasma jet.

The OES analysis confirms that no reactive atoms could be generated, which means the current CE–MIP is not able to etch silicon materials. It should be considered that the internal fused quartz tube acts as a sink for the reactive fluorine species: Some of the fluorine will etch the fused quartz tube. Then, considering that the highest energy region of the plasma was inside the plasma torch, the relatively low microwave power of 15 W and the gas flow rate of 1 L/min will have resulted in relatively low energy plasma discharging from the nozzle. These effects, it is concluded, are the reason that no fluorine emission lines were detected.

The injection of a secondary argon gas flow into the argon plasma jet showed an interesting aspect of the CE–MIP torch with the bespoke nozzle attached. The secondary argon gas flowed at 1% of the main gas flow value. However, Fig. 9 shows that this resulted in an increase of the relative intensity of the 801.5 nm photons by 9%. This is a significant result, which should be investigated further. The microwave electric field coupled into the surface layers of the plasma, in accordance with the skin effect [33]; and, as the secondary gas was injected directly into the surface layer region of the plasma jet, it is concluded that this was the cause of the increase in the photonic intensity, which would be due to an increase in the degree of ionisation within the plasma [34].

The future work on the CE–MIP development will be focused on increasing the power from 15 W to over 80 W, and the increased energy is expected to ionise reactive particles for etching applications.

6 Conclusions

The adaptation of a characterisation process capable of mapping the microwave energy going into the plasma and the resulting photonic energy distribution within the plasma has been developed. This process was used to characterise a CE–MIP torch that was modified with a bespoke nozzle designed to inject secondary gases downstream of the main plasma jet. Microwave spectrum analysis and OES analysis were carried out to characterise the modified CE–MIP troch, which was finally tested in the experiment on glass surface modification. The conclusions can be drawn as follows:

1) A polar plot of the microwave energy being emitted from the coaxial electrode is developed by microwave spectrum analysis. It is proven to be more advantageous than vector network analysis, providing detailed information on the microwave electric field in the CE–MIP torch.

2) Photonic intensity spatial maps are generated by recording the intensities of the different photons emitted at locations across the entire plasma jet. Significant increase (circa 9%) of energy is recorded for only a 1% increase of additional argon feed into the bespoke nozzle. OES analysis confirms that no reactive atoms could be generated by injecting reactive gases.

3) The CE–MIP torch successfully modified the surface energy of CSP glass. A super-hydrophilic surface is evidenced by the change in water contact angle from circa 57° to as small as 1°. The stability of the torch is tested using OES and repeatable surface processing results (with deviation of 0.5°) are demonstrated for the MIP torch over a 12-h period.

Acknowledgements This research work was funded by the Centre for Innovative Manufacturing in Ultra Precision of the Engineering and Physical Sciences Research Council, UK (Grant No. EP/I033491/1), the Centre for Doctoral Training in Ultra Precision Engineering of the Engineering and Physical Sciences Research Council, UK (Grant No. EP/K503241/1), the Science Foundation Ireland (SFI) (Grant No. 15/RP/B3208), Irish Research Council (Grant No. CLNE/2018/1530), and the National Natural Science Foundation of China (Grant No. 51705462). The authors would also like to thank ADTEC Plasma Technology & ADTEC Europe for providing financial and technical support, and bespoke plasma equipment. Finally, our appreciation is given to Cranfield University for the use of their facilities and to their following staff who supported different aspects of this work: Dr. Renaud Jourdain, Prof. Jose Endrino, Prof. Chris Sansom, Prof. John Nicholls, and Prof. Paul Shore.

References

1. Yu N, Liu J, Mainaud Durand H, et al. Mechanically enabled two-axis ultrasonic-assisted system for ultra-precision machining. Micromachines, 2020, 11(5): 522

2. Yang X, Yang X, Sun R, et al. Obtaining atomically smooth 4H–SiC (0001) surface by controlling balance between anodizing and polishing in electrochemical mechanical polishing. Nanomanufacturing and Metrology, 2019, 2(3): 140–147
3. Jourdain R, Castelli M, Yu N, et al. Estimation of the power absorbed by the surface of optical components processed by an inductively coupled plasma torch. Applied Thermal Engineering, 2016, 108: 1372–1382
4. Czotscher T, Wielki N, Vetter K, et al. Rapid material characterization of deep-alloyed steels by shock wave-based indentation technique and deep rolling. Nanomanufacturing and Metrology, 2019, 2(1): 56–64
5. Castelli M, Jourdain R, Morantz P, et al. Rapid optical surface figuring using reactive atom plasma. Precision Engineering, 2012, 36(3): 467–476
6. Arnold T, Böhm G, Paetzelt H. Nonconventional ultra-precision manufacturing of ULE mirror surfaces using atmospheric reactive plasma jets. Proceedings Volume 9912, Advances in Optical and Mechanical Technologies for Telescopes and Instrumentation II, 2016, 99123N
7. Sun R, Yang X, Watanabe K, et al. Etching characteristics of quartz crystal wafers using argon-based atmospheric pressure CF_4 plasma stabilized by ethanol addition. Nanomanufacturing and Metrology, 2019, 2(3): 168–176
8. Williams C B, Amais R S, Fontoura B M, et al. Recent developments in microwave-induced plasma optical emission spectrometry and applications of a commercial Hammer-cavity instrument. TrAC Trends in Analytical Chemistry, 2019, 116: 151–157
9. Selezneva S E, Boulos M I. Supersonic induction plasma jet modeling. Nuclear Instruments & Methods in Physics Research. Section B, Beam Interactions with Materials and Atoms, 2001, 180(1–4): 306–311
10. Stephan A, Heuermann H, Prantner M. Cutting human tissue with novel atmospheric-pressure microwave plasma jet. In: Proceedings of the 46th European Microwave Conference (EuMC). London: IEEE, 2016, 902–905
11. Hattori Y, Mukasa S, Nomura S, et al. Optimization and analysis of shape of coaxial electrode for microwave plasma in water. Journal of Applied Physics, 2010, 107(6): 063305
12. Williams D F, Kellar E J, Jesson D A, et al. Surface analysis of 316 stainless steel treated with cold atmospheric plasma. Applied Surface Science, 2017, 403: 240–247
13. Mariotti D, Sankaran R M. Microplasmas for nanomaterials synthesis. Journal of Physics. D, Applied Physics, 2010, 43(32): 323001
14. Karanassios V. Microplasmas for chemical analysis: Analytical tools or research toys? Spectrochimica Acta. Part B, Atomic Spectroscopy, 2004, 59(7): 909–928
15. Sakai O, Tachibana K. Plasmas as metamaterials: A review. Plasma Sources Science & Technology, 2012, 21(1): 013001
16. Starikovskaia S M. Plasma assisted ignition and combustion. Journal of Physics. D, Applied Physics, 2006, 39(16): R265–R299
17. Barbieri D, Boselli M, Cavrini F, et al. Investigation of the antimicrobial activity at safe levels for eukaryotic cells of a low power atmospheric pressure inductively coupled plasma source. Biointerphases, 2015, 10(2): 029519
18. von Engel A. Ionized Gases. New York: American Institute of Physics, 1994
19. Stonies R, Schermer S, Voges E, et al. A new small microwave plasma torch. Plasma Sources Science & Technology, 2004, 13(4): 604–611
20. Li D, Tong L, Gao B, et al. The study of 2.45 GHz atmospheric microwave plasma generator. In: Proceedings of the 6th International Symposium on Microwave, Antenna, Propagation, and EMC Technologies (MAPE). Shanghai: IEEE, 2015, 628–632
21. Helfrick A D. Electrical Spectrum and Network Analyzers: A Practical Approach. Salt Lake City: American Academic Press, 2012
22. Hammerstad E O. Microstrip Handbook. Trondheim: Electronics Research Laboratory, University of Trondheim, Norwegian Institute of Technology, 1975
23. Zheng Z, Chen Z, Liu P, et al. Study on argon plasma jets at atmospheric pressure in ambient air excited by surface waves. IEEE Transactions on Plasma Science, 2014, 42(4): 911–916
24. Ono R. Optical diagnostics of reactive species in atmospheric-pressure nonthermal plasma. Journal of Physics. D, Applied Physics, 2016, 49(8): 083001
25. Bennett A, Sansom C, King P, et al. Cleaning concentrating solar power mirrors without water. In: Proceedings of AIP Conference. AIP, 2020
26. Bennett A, Jourdain R, MacKay P, et al. Processing of crystal quartz using atmospheric pressure microwave plasma technology. In: Proceedings of the 18th International Conference of European Society for Precision Engineering & Nanotechnology. Venice, 2018
27. Harvey A F. Standard waveguides and couplings for microwave equipment. Proceedings of the IEE-Part B: Radio and Electronic Engineering, 1955, 102(4): 493–499
28. Yu N, Jourdain R, Gourma M, et al. Analysis of De-Laval nozzle designs employed for plasma figuring of surfaces. International Journal of Advanced Manufacturing Technology, 2016, 87(1–4): 735–745
29. Yu N, Yang Y, Jourdain R, et al. Design and optimization of plasma jet nozzles based on computational fluid dynamics. International Journal of Advanced Manufacturing Technology, 2020, 108(7–8): 2559–2568
30. Balanis C A. Antenna Theory: Analysis and Design. New York: John Wiley & Sons, 2016
31. Timmermans E A, Jonkers J I, Thomas I A, et al. The behavior of molecules in microwave-induced plasmas studied by optical emission spectroscopy. 1. Plasmas at atmospheric pressure. Spectrochimica Acta. Part B, Atomic Spectroscopy, 1998, 53(11): 1553–1566
32. Wang W, Murphy A B, Rong M, et al. Investigation on critical breakdown electric field of hot sulfur hexafluoride/carbon tetrafluoride mixtures for high voltage circuit breaker applications. Journal of Applied Physics, 2013, 114(10): 103301
33. Gustrau F. RF and Microwave Engineering: Fundamentals of Wireless Communications. New York: John Wiley & Sons, 2012
34. Hutchinson P I, Freidberg P J. Introduction to Plasma Physics I. New York: Springer, 2003